

High-Temperature Erosion Resistance of FeBSiNb Amorphous Coatings Deposited by Arc Spraying for Boiler Applications

J.B. Cheng, X.B. Liang, Y.X. Chen, Z.H. Wang, and B.S. Xu

(Submitted September 7, 2012; in revised form November 20, 2012)

Erosive high-temperature wear in boilers is one of the main causes of downtime and one of the principal engineering problems in these installations. This article discusses the use of FeBSiNb amorphous coatings synthesized by arc spraying to improve elevated-temperature erosion resistance for boiler applications. The influence of test temperature, velocity, and impact angle on material wastage was revealed using air solid particle erosion rig. The experimental results showed that moderate degradation of the coating was predominant at lower impact velocity and impact angles, while severe damage arose for higher velocities and impact angles. The erosion behavior of the coating was sensitive to test temperature. The erosion rates of the coating decreased as a function of environment temperature. The relationship between microstructure and erosion resistance of the coating was also analyzed in details. The FeBSiNb coating had excellent elevated-temperature erosion resistance at temperatures at least up to 600 °C during service.

Keywords amorphous structures, arc spray, boiler materials, erosion resistance

1. Introduction

In recent years, there has been increasing attention paid to the energy-conversion efficiency of power plants to meet the need of industries along with ensuring plant reliability, availability, and maintainability. All design parameters of plants are focused on obtaining the maximum life of the boiler and boiler tubes, maximum thermal efficiency, low NO_x emissions, and maximum power generation (Ref 1-3). However, erosive high-temperature wear by fly ash particles in boilers is one of the main causes of downtime and one of the principal engineering problems in these installations. Maintenance costs for replacing broken pipes in the same installations are also very high and can be estimated at up to 54% of the total production costs (Ref 4). The downtime associated with unscheduled breakdowns caused by the failure of exchange tubes is a source of lost revenue. Therefore, the development of elevated-temperature erosive-wear

protection systems in industrial boilers is an extremely important topic from both engineering and economic perspectives. Thermal spray coatings are an alternate approach that offers advantages because they allow in situ recoating of the boiler tubes with the additional ability to repair localized defects inside the boiler. Arc spraying is considered a simple, low-cost, highly efficient coating process. The ability to recoat boilers during a scheduled outage is especially attractive because downtime can be minimized, which translates into significant operational cost savings.

Several types of thermal sprayed coatings are used in erosion conditions, including iron aluminum (Ref 5), nickel aluminum (Ref 6), nickel chrome (Ref 7), titanium aluminum (Ref 8), and Praxair Surface Technologies' proprietary ultrahard iron-based wires. Recently some significant efforts have been made to develop amorphous and nanoscale coatings because of their superior mechanical and chemical properties compared with conventional crystalline structure. Many papers investigate wear and erosion performance of arc sprayed nanoscale coatings. The NanoSteel Company reports two nanocomposite coatings that were formed from iron-based amorphous alloys, SHS7170 and SHS8000, using conventional twin wire-arc spraying technology (Ref 9, 10). When heated to temperatures above its peak crystallization temperature, the as-sprayed coatings contain iron-based amorphous matrix with nanoscale carbides and borides. The coatings have demonstrated high performance during elevated-temperature erosion testing. Georgieva et al. (Ref 11) developed TAFA 140MXC cored wires to deposit nanocrystalline coatings using arc spraying process. In the past few years, FeCrBSiMnNbY and FeCrBSiNbW metallic glass coatings have been successfully prepared by arc spraying in our laboratory (Ref 12, 13).

J.B. Cheng, College of Mechanics and Materials, Hohai University, Nanjing 210098, China; and National Key Laboratory for Remanufacturing, Academy of Armored Forces Engineering, Beijing 100072, China; **Z.H. Wang**, College of Mechanics and Materials, Hohai University, Nanjing 210098, China; and **X.B. Liang**, **Y.X. Chen**, and **B.S. Xu**, National Key Laboratory for Remanufacturing, Academy of Armored Forces Engineering, Beijing 100072, China. Contact e-mail: chengjiangbo@hotmail.com.

The microstructures of both coatings consist of amorphous matrix embedded with $\alpha(\text{Fe,Cr})$ nanocrystalline particles. The as-sprayed coating has been confirmed to possess high hardness, low wear rate, and improved corrosion resistance. In this study, a more recent FeBSiNb amorphous coating was developed. Compared with the previous FeCr-based amorphous coatings, the FeBSiNb coating has enhanced glass-forming ability, which allows the formation of a primary amorphous matrix upon initial spraying. The novel FeBSiNb amorphous coatings are believed to have a considerable potential for elevated-temperature environments involving erosion engineering applications because of their advantageous properties and low cost.

To explore the possibility of preparing amorphous coatings by thermal spraying conventional feedstock wires, an exploratory study on the multicomponent FeBSiNb metallic glass coatings produced by arc spraying was carried out in the present work. The microstructures of the coatings were characterized. The porosity and microhardness were examined. The erosion performance of the coating was evaluated with a laboratory elevated-temperature erosion tester. The effects of the different parameters, such as particle velocity, impact angles, and environment temperature, on the erosion properties of the coatings were studied in details. The relationship between erosion behavior and the structure of the coatings was analyzed.

2. Experimental Procedures

2.1 Materials

A self-designed Fe-base cored wire (Fe-B-Si-Nb) with diameter of 2 mm was used as feedstock. The chemical composition of the cored wire is listed in Table 1. Mild steel, which is often used to fabricate boiler tubes, was used as a substrate for the FeBSiNb coating. The chemical composition of the mild steel is listed in Table 2. The bare steel was also subjected to the erosion test for comparison.

2.2 Deposition of the Coating

Prior to spraying, the nonsprayed surface of mild steel substrate ($25 \times 16 \times 5 \text{ mm}^3$) was treated by powder calorizing (powder: 15% Al, 84% Al_2O_3 , 0.5% NH_4Cl , and 0.5% KHF_2 ; process condition: $900 \text{ }^\circ\text{C} \times 4 \text{ h}$) to reduce the effect of oxidation at high temperature on the erosion test. Prior to coating, the sprayed surface of the substrate was degreased by acetone, dried in air, and then grit blasted. A wire-arc gun system was used for coating preparation (JZY-250, Beijing Jiazhiyuan Scientific & Trading Co., Ltd., China). The arc spray process parameters are shown in Table 3.

Table 1 Composition of the cored wire

	Composition, wt. %			
	B	Si	Nb	Fe
Cored wires	2-6	1-4	4-9	Bal

2.3 Characterization of the Coating

The microstructure of the coating was characterized using scanning electron microscopy (SEM) with energy dispersive x-ray analysis (EDAX) (Philips Quant 200 and S3400), x-ray diffraction (XRD) (D8-Advance with Cu-K α radiation), and high-resolution transmission electron microscopy (HRTEM). The image analysis method was used for the measurement of porosity, at a magnification of $500\times$ with a minimum sample size of 20. The microhardness profile along the depth direction of the coating was evaluated by the Vickers hardness tester (HV-1000, Jinan Precision Testing Equipment Co., Ltd., China) with a testing load of 1.96 N and a dwelling of 15 s.

2.4 Erosion Test

The erosion tests were carried out by means of a gas bed ash elevated-temperature erosion apparatus equipped in National Key Laboratory for Remanufacturing (Academy of Armored Forces Engineering, Beijing). It consists of five parts: blasting system, heating system, abrasive blender, erosion room, and temperature-controlling system. The diagrammatic sketch of the elevated-temperature erosion apparatus is shown in Fig. 1. Samples of the same lot of feedstock bed ash were used for all of the high-temperature erosion tests and consisted of particles that were mainly angular in shape with a particle size ranging from 63 to 300 μm . Using EDAX analysis, the particles of bed ash were found to contain oxide particles with high concentrations of Si, and minor concentrations of Al, Ca, S, Fe, K, Ti, and Cl. The compositional analysis is consistent with the normal constituents of ash (SiO_2 , Al_2O_3 , CaO, SO, Fe_2O_3 , KO_2 , and TiO_2), which have been identified elsewhere (Ref 4). Note that while fly ash contacts with higher velocity, it is smaller in size and generally less erosive than bed ash.

To eliminate the effect of surface conditions, all test pieces were polished before the erosion test. Before being submitted to the erosion test, specimens were heated to the test temperatures over a period of time of about 15 min. The bed ash and gas were heated simultaneously.

Table 2 Chemical compositions of the mild steel for boiler tube

Element	Composition, wt. %
C	0.17-0.24
Si	0.17-0.37
Mn	0.35-0.65
S	≤ 0.035
P	≤ 0.035

Table 3 Parameters of wire arc spraying process

Parameter	Value
Spraying voltage, V	36
Wire feed rate, m/min	2.9
Compressed air pressure, kPa	700
Standoff distance, mm	200

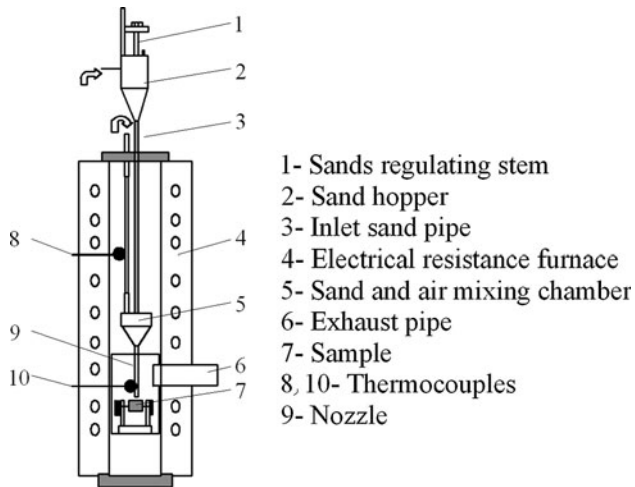


Fig. 1 Elevated-temperature erosion apparatus

Table 4 Erosion test parameters

Parameter	Value
Temperature, °C	300, 450, 600
Impact angle, °	30, 90
Ash feeding, g/per	375
Test duration, h	0.5
Particle velocity, m/s	60, 90, 110

The bed ash velocity was set by air pressure as the velocity at different air pressures had been determined by air compressor. The impingement angle was adjusted by rotating the sample. Temperature was measured by E-type thermocouples placed at a location beside the specimens. The parameters used in these erosion tests, which include temperature, impact angle, erodent feeding rate, testing time, and gas velocity, are given in Table 4. Under each test condition, three test pieces were used and the erosion rate was the average of three tests.

The mass loss was determined by weighing the samples before and after the test using a precision electronic balance with an accuracy of 0.1 mg. The erosion rate ε (mg/g) was determined by:

$$\varepsilon = \frac{M_1}{M_2} \quad (\text{Eq 1})$$

where M_1 (mg) is the mass loss of the sample and M_2 (g) is the mass of erosion bed ash.

After erosion, the patterns and compositions of the eroded surface were also investigated by SEM, EDAX, and XRD.

3. Results

3.1 Microstructure Characterization

Figure 2 shows the cross-sectional microstructure of the arc sprayed FeBSiNb coating. The coating thickness was about 700 μm . It was very dense and smooth, adhering

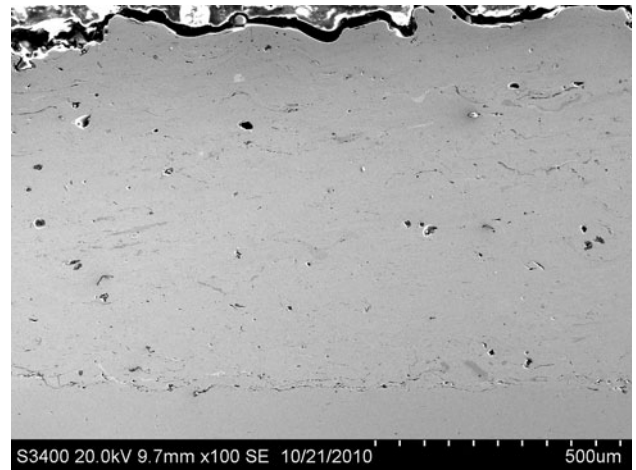


Fig. 2 SEM image of the coating

Table 5 Chemical composition of the coating

	Composition, at.%			
	B	Si	Nb	Fe
Coating	17.95	1.64	2.08	bal

well to the substrate with no cracking. Some pores are visible as very dark regions. In some sections, the coating appears quite smooth and more similar to a bulk material than to a sprayed coating. The average porosity of the coating was determined to be 1.2% (the value range was 0.9-1.7%) by image analysis. The chemical compositions of the coating are listed in Table 5.

The featureless HRTEM image and corresponding selected-area electron diffraction (SAED) with pattern typical for an amorphous structure are shown in Fig. 3 and the inset. It was therefore concluded that the FeBSiNb coating originates from the glassy structure.

Figure 4 shows the variation of microhardness of the coating as a function of erosion test temperature. The average Vickers hardness of the as-sprayed coating was 1075 $\text{HV}_{0.1}$ (the value range was 1054-1094 $\text{HV}_{0.1}$). The highest microhardness value of the coating reached 1381 $\text{HV}_{0.1}$ (the value range was 1358-1394 $\text{HV}_{0.1}$) at test temperature of 600 °C. The reason is that when recrystallization process takes place at higher temperatures, nanoscale grains appear and act as dispersion strengtheners, so hardness clearly increases. The result is verified by XRD patterns in the discussion.

3.2 Erosion of the Coating and Mild Steel

Figure 5 shows the erosion rates of mild steel and the coating as a function of particle velocity with impact angle at 30° and temperature of 25 °C. The erosion rates of both samples increased with the increase in velocity. Compared with mild steel, the coating had lower erosion rates under

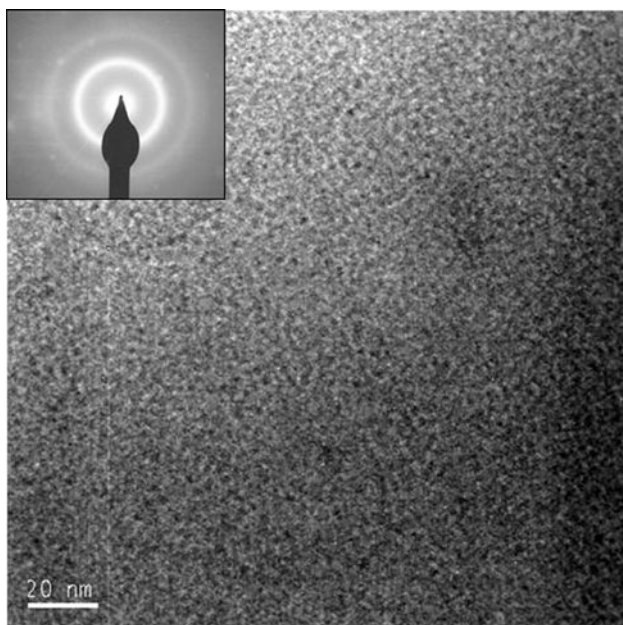


Fig. 3 HRTEM images of the coating. Inset SAED pattern shows diffuse rings

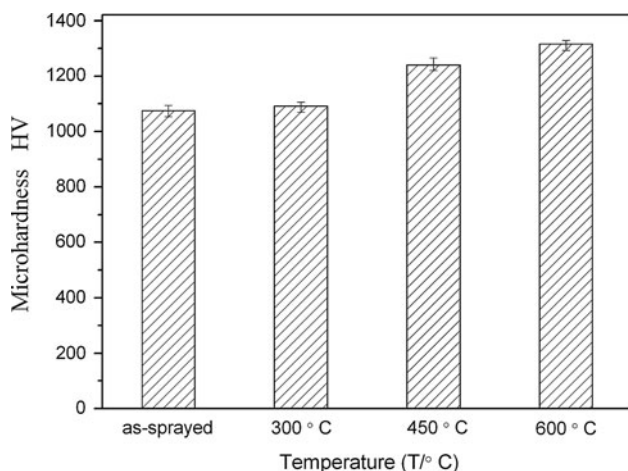


Fig. 4 Vickers hardness profile of the coating with different test temperature

the same testing conditions, indicating that the coating presented better erosion resistance. Erosion rate has been shown (Ref 14, 15) to follow an empirical power law relationship with velocity:

$$\varepsilon = K v^n \quad (\text{Eq } 2)$$

where ε is erosion rate, v is velocity, K is a constant, and n has values between 2 and 3.5 for metallic materials. Brittle materials tend to have a larger n range, from 2 to 6.5 (Ref 14). According to the experimental results, the n value is 2.8 for the FeBSiNb coating and 2.1 for mild steel. Therefore, the tested samples had a higher erosion resistance with the lower particle velocity. In addition, the n value of the coating was larger than that of mild steel,

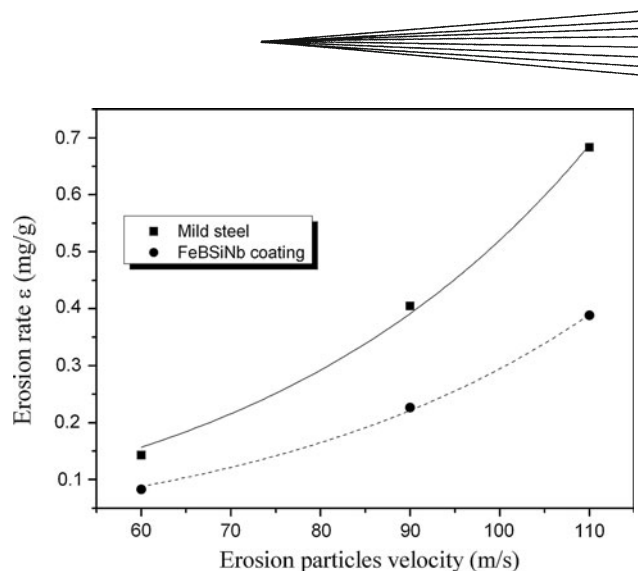


Fig. 5 Erosion rates of the mild steel and the coating as function of velocity with impact angle at 30° and room temperature

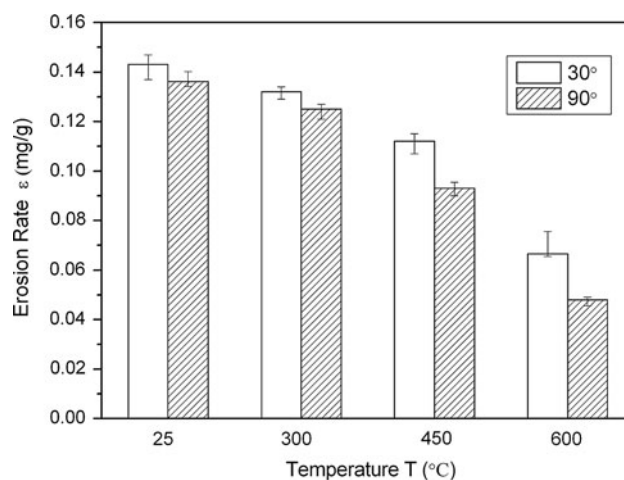


Fig. 6 Effect of erosion temperature and impact angle on the erosion rate of mild steel

indicating that erosion rate of the coating was very sensitive to slight changes in erodent particles.

Figure 6 shows the effect of test temperatures and impact angles on the erosion rate of the mild steel with particle velocity of 60 m/s. The erosion rate significantly decreased as a function of the test temperature at impact angles of both 30 and 90°. At the test temperature of 600 °C, the erosion rate at 30° was nearly 1.5 times higher than that at 90°. According to the erosion theory of ductile metallic materials, the erosion rate of metals becomes the maximum at impact angle range from about 15° to 20° (Ref 16). It decreases with the increase of impact angle. Therefore, the erosion rate of the mild steel tested at 30° impact angle was higher than that at 90° under all test temperatures. This means that the mild steel exhibited better erosion resistance at higher impact angle.

However, the effect of impact angles on the erosion rate of the coating exhibited a reverse trend as function of test temperature, as shown in Fig. 7. Namely, the coating

exhibited better erosion resistance at lower impact angle. At the test temperature of 600 °C, the erosion rate of the coating at 90° was nearly 2 times higher than that at 30°. Moreover, the erosion rate of the coating decreased as a

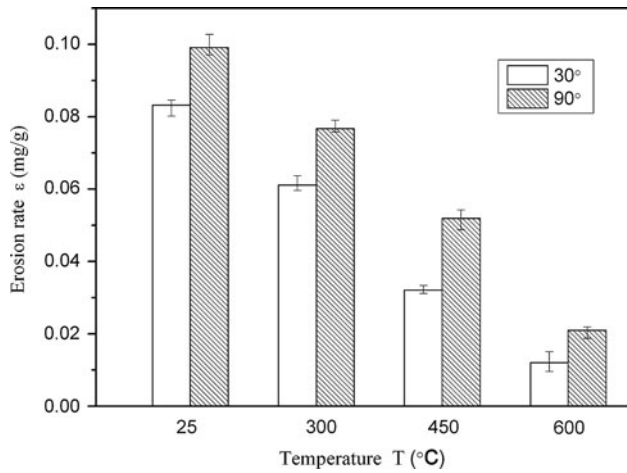


Fig. 7 Effect of erosion temperature and impact angle on the erosion rate of the FeBSiNb coating

function of test temperature with impact angles of both 30 and 90°. At the impact angle of 30°, the erosion rate of the coating at 25 °C was nearly 7 times higher than that at 600 °C. Moreover, the relatively erosion resistance of the coating at 600 °C was about 5.5 and 2.3 times higher than the mild steel at the impact angles of 30 and 90°, respectively. That suggests that the coating had excellent elevated-temperature erosion resistance.

4. Discussion

From Fig. 6 and 7, it can be seen that the mild steel displayed the main effects at low impingement angle, while the FeBSiNb coating showed main effects at high impingement angle. Equation 3 is mostly used to express the erosion rate at different angle (Ref 17):

$$\varepsilon = A \cos^2 \beta \sin(n\beta) + B \sin^2 \beta \quad (\text{Eq 3})$$

where ε is the erosion rate, β is the impingement angle, n is a constant, and A and B are also constants to describe the brittle and plastic behavior, respectively. For typical brittle material $A=0$, for typical plastic material $B=0$, and for the other material, the plastic item displays the main

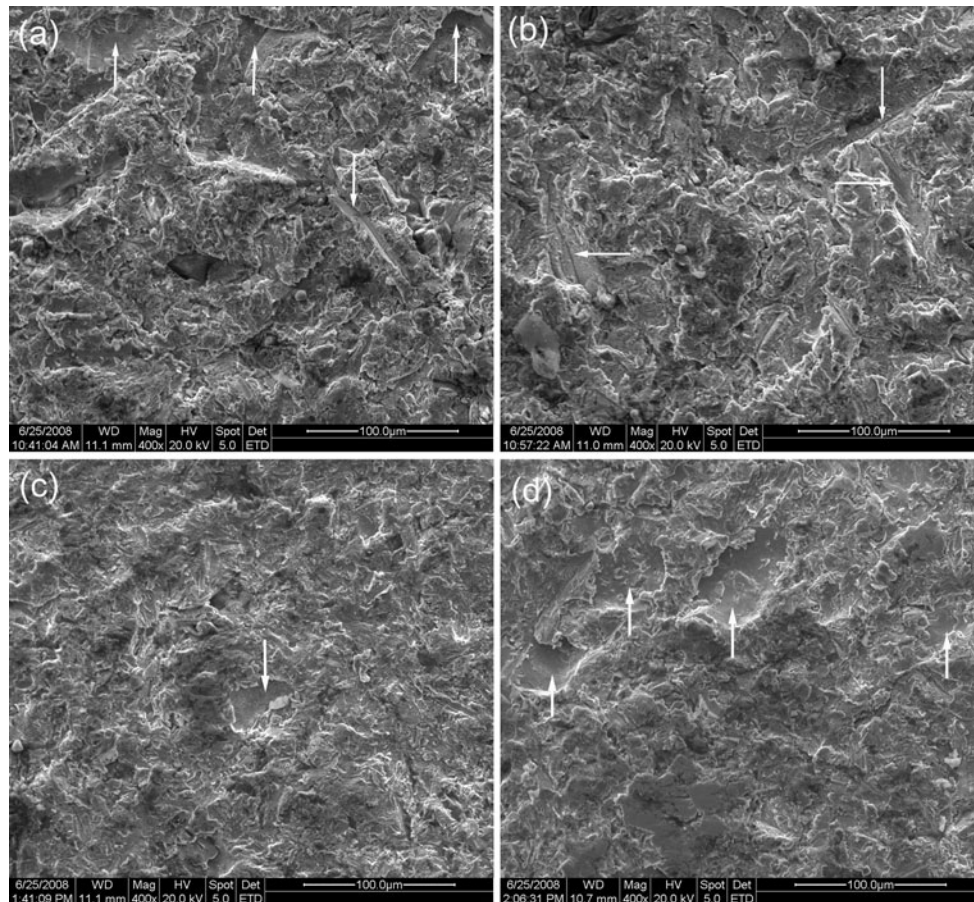


Fig. 8 Eroded surfaces of mild steel and the coating (a) 30° impact angle and (b) 90° impact angle of the mild steel, (c) 30° impact angle and (d) 90° impact angle of the coatings, respectively

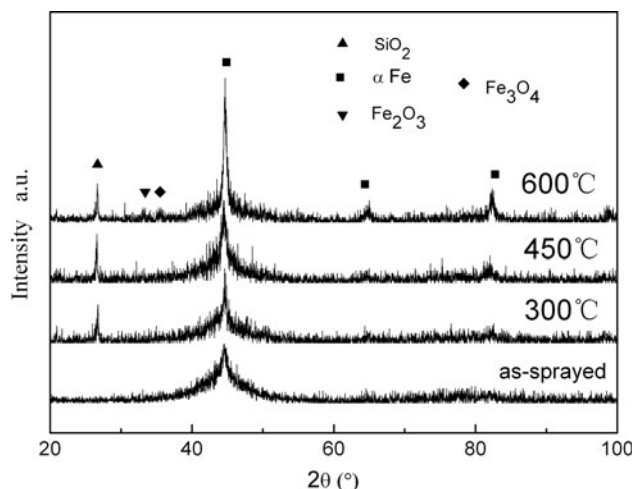


Fig. 9 XRD patterns of the tested coatings

Table 6 EDAX values of worn surface coating with different temperatures

Temperature, °C	Composition, at.%				
	O	B	Si	Nb	Fe
300	6.91	25.05	2.97	2.31	62.76
450	8.82	29.93	1.75	1.77	57.73
600	13.13	28.99	1.01	2.27	54.61

effects at low impingement angle while the brittle item does so at high impingement angle. That is, the brittle materials have high erosion rate at high impingement angle, but low erosion rate at low impingement angle, and it is reversed for plastic materials (Ref 17). This is consistent with the high hardness of the coating and its ability to resist the cutting or ploughing mechanism of impinging particles impacting at low angle. At higher angle, the kinetic energy of the impinging particles is transferred directly to the coating, and material removal occurs by the formation of cracks (Ref 9).

The eroded surfaces of the test coating and the mild steel are presented in Fig. 8. Figure 8(a) and (b) show the eroded surfaces of the mild steel at different impact angles at test temperature of 25 °C. There is evidence of “ploughing” or “cutting” on the erosion surface (see arrows as in Fig. 8a and b). This process occurs when the high-speed erosion particles embed into the surface of the mild steel and act as fixed indenters, causing the so-called grooving wear mode. For the mild steel eroded at 30° impact angle, severe scuffing and big pits were present in the worn surface. For ductile mild steel, at lower impact angle, the sample surface was sloped. The high-speed particles attacked the surface for a long time. These pits were formed by the impact of successive erosion particles. The entire worn surface was quite rough. It corresponded to larger erosion loss. However, the eroded sample at 90° impact angle had a smoother surface morphology than

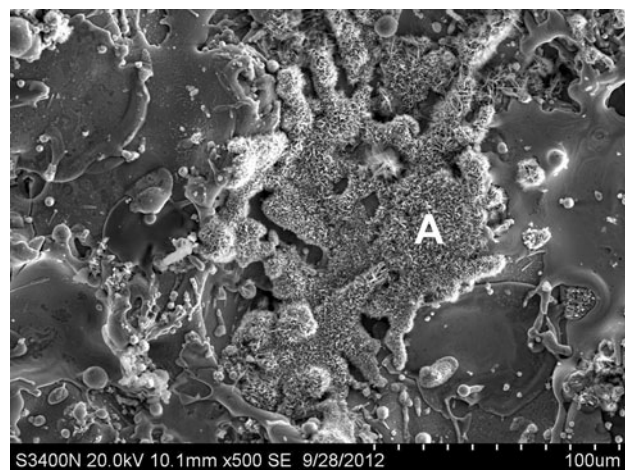


Fig. 10 SEM image of the noneroded surface of the coating at test temperature of 600 °C

that at 30°. Only some shallow “ploughings” existed in the worn surface. The particles acted on the sample surface for a short time due to plane shape. It bruised the sample surface, and slight scratching was present on the worn surface. Therefore, cutting and ploughing were the main abrasive wear mechanisms. Figure 8(c) and (d) show eroded surfaces of the coating at 30 and 90° impact angles at test temperature of 25 °C. For FeBSiNb coatings, free “ploughing” or “cutting” appeared on the worn surface. Only typical crater or void morphologies are seen in the eroded surface (see arrows in Fig. 8c and d). Compared with the coating eroded at 30° impact angle, parts of coatings were chipped off and coarse craters morphology were present at 90°. The coating at 90° impact angle absorbed greater impact energy than that at 30° angle because of the plane surface. For brittle coatings, it leads to brittle failure. It accounts for their higher erosion wastage than that of erosion at lower impact angles. During erosion, the deformation of coating takes place between splats initially. It generates microcracks and forms small craters, which causes slight erosion wastage. As the test proceeds, the initial microcracks propagates during subsequent attacks by erodent particles (Ref 18). Parts of fractured and loosened pieces of the coating appear in the surface coating. These pieces are chipped off by successive particle attacks. Finally, many small craters and voids form (Ref 19). This is also termed cracking and chipping brittle mechanism.

It is evidently found that the erosion rates of the coating decreased with the increase of test temperature at impact angles of both 30 and 90°. This is attributed to three factors. Erosion, like any wear process, is a dynamic process. It is related to the formation of microstructures (including phase, grain size, texture etc.) and their changes (including new phase formation, glass to crystalline transformation, etc.) during erosion testing (Ref 20). Firstly, more and more nanoscale grains are precipitated in the coatings with increasing erosion temperatures. Figure 9 shows the XRD patterns of the coatings after

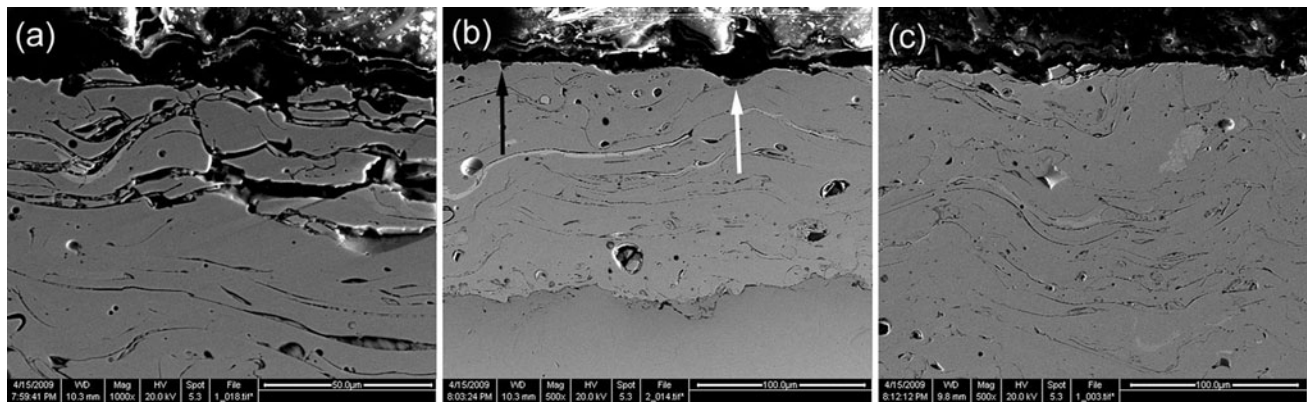


Fig. 11 Cross-section morphologies of the coatings after erosion test at impact angle of 30° and temperature of (a) 25 °C, (b) 450 °C, and (c) 600 °C

erosion testing. The intensity of the x-ray diffraction peaks is increased, and the XRD curves at $2\theta = 43.5^\circ$ become narrower and narrower with increasing test temperature. The FWHM values of the coating analyzed by XRD were 0.918988, 0.6779664, and 0.5893521 for test temperatures from 300 to 600 °C, respectively. The FWHM values of the coating became smaller and smaller as a function of test temperature. This means that the nanoscale grain formed in the coating. Those finer nanocrystalline grains improved the microhardness of the coating, as shown in Fig. 4. The coating with higher hardness could have prevented the material removal during erosion. Secondly, the other explanation for the behavior is related to the formation of a thick oxide at elevated temperatures that reduced the erosion rate of the material. When a thick oxide scale exists, erosion takes place from the scale only (Ref 21). The chemical compositions of the worn surface coating as a function of test temperature are listed in Table 6. The oxygen content of the coating increased with increasing test temperature. Figure 10 shows the SEM image of the noneroded surface of the coating at test temperature of 600 °C. It can be seen that local needle-like oxides formed on the surface coating. The chemical compositions in A zone of the coating were 55.63O-3.65Si-2.02Nb-38.7Fe (at.%). Additional information from the XRD analysis showed the oxides on the surface coating are Fe_2O_3 and Fe_3O_4 . When hard particles impacted the sample surface, the surface of eroded sample showed a typical flaky appearance because of the cracking and spalling of the oxide scale. The erosion process of the sample is a repeat process of formation-crack-spalling-formation of oxide scale (Ref 22). Thirdly, the reason for the coatings with excellent erosion resistance is mainly related to the weight gain produced by oxidation and erodent ash particles embedment in the surfaces of the coatings. From Fig. 9, the peaks of SiO_2 exist in XRD patterns as function of erosion temperature. Such embedment would modify the surface of the coatings, reducing their erosion rates after an initial “running in.” Therefore, the coatings provided significant erosion resistance and protection over a wide temperature range.

Figure 11 shows the cross-sectional morphologies of the coating after erosion test with different test temperatures and impact angle at 30°. Numbers of intersplat cracks can be clearly observed near the coating surface at temperature of 25 °C, as shown in Fig. 11(a). This is attributed to the impact of the erosion particles on the coating surface. The lamellar coating was formed by a large amount of small splat deposition. The adjacent two splats were bonded partially, and a significant nonbonded area existed between the two splats. The nonbonded area acted as a precrack, which propagated under the impact of erosive particles on the coating surface. Consequently, before the splat was completely attacked by erosive fly ash particles, the crack propagation originating from the nonbonded interface area may have led to the flaking of one splat or several splats. Figure 11(b) and (c) are SEM images of the coating at test temperatures of 450 and 600 °C, respectively. It can be seen that the surface of the coating became smooth as function of test temperature. A pit morphology marked with a large white arrow is visible in the coating at test temperature of 450 °C, as shown in Fig. 11(b). In addition, the groove marked with black arrow appeared in the eroded surface (Fig. 11b). It has caused the transition of erosion mechanism from a purely “brittle” to a relatively “ductile” behavior (Ref 20). This transition is mainly related to the change in the strength and ductility of material with increasing temperature (Ref 20). However, the predominant erosion mechanism was brittle fracture. When the erosion temperature reached 600 °C, few microcracks and small pits were observed in the coating, as shown in Fig. 11(c). This confirms that the smaller splats were chipped off from the coating. Therefore, the coating had excellent elevated erosion resistance.

5. Conclusions

The erosion performance of the arc sprayed FeBSiNb amorphous coating and mild steel at temperatures from 25 to 600 °C was investigated using bed ash as erodent. Results showed that the erosion rates of the coating



increased as function of velocity. The coating exhibited the lower erosion rate at 30° impact angle. The erosion rate of the coating decreased with increasing of the test temperature at the erosion angles of both 30 and 90°. The relative erosion resistance of the coating at 600 °C was about 5.5 and 2.3 times higher than the mild steel at the impact angles of 30 and 90°, respectively. The mass loss of the coating was attributed to splat flaking on the surface. The primary failure mechanism of the coatings was brittle fracture. The arc sprayed FeBSiNb amorphous coating had excellent elevated erosion resistance. The universal ability of the FeBSiNb coatings to serve at erosion temperatures at least up to 600 °C was important for real-world boiler applications.

Acknowledgments

The authors are grateful for support provided by Natural Science Foundation of China (51105129).

References

1. A. Gungor and N. Eskin, Two-Dimensional Coal Combustion Modeling of CFB, *Int. J. Therm. Sci.*, 2008, **47**, p 157-174
2. V. Kain, K. Chandra, and B.P. Sharma, Failure of Carbon Steel Tubes in a Fluidized Bed Combustor, *Eng. Fail. Anal.*, 2008, **15**, p 182-187
3. M.B. Gandhi, R. Vuthaluru, H. Vuthaluru, D. French, and K. Shah, CFD Based Prediction of Erosion Rate in Large Scale Wall-Fired Boiler, *Appl. Therm. Eng.*, 2012, **42**, p 90-100
4. V.H. Hidalgo, F.J.B. Varela, and E.F. Rico, Erosion Wear and Mechanical Properties of Plasma-Sprayed Nickel- and Iron-Based Coatings Subjected to Service Conditions in Boilers, *Tribol. Int.*, 1997, **30**, p 641-649
5. X.Q. Yu, M. Fan, and Y.S. Sun, The Erosion-Corrosion Behavior of Some Fe₃Al-Based Alloys at High Temperatures, *Wear*, 2002, **253**, p 604-609
6. S.B. Mishra, K. Chandra, S. Prakash, and B. Venkataraman, Characterisation and Erosion Behaviour of a Plasma Sprayed Ni₃Al Coating on a Fe-Based Superalloy, *Mater. Lett.*, 2005, **59**, p 3694-3698
7. N. Espallargas, J. Berget, J.M. Guilemany, A.V. Benedetti, and P.H. Suegama, Cr₃C₂-NiCr and WC-Ni Thermal Spray Coatings as Alternatives to Hard Chromium for Erosion-Corrosion Resistance, *Surf. Coat. Technol.*, 2008, **202**, p 1405-1417
8. S.G. Liu, J.M. Wu, S.C. Zhang, S.J. Rong, and Z.Z. Li, High Temperature Erosion Properties of Arc-Sprayed Coatings Using Various Cored Wires Containing Ti-Al Intermetallics, *Wear*, 2007, **262**, p 555-561
9. D.J. Branagan, M. Breitsameter, B.E. Meacham, and V. Belashchenko, High-Performance Nanoscale Composite Coatings for Boiler Applications, *J. Therm. Spray Technol.*, 2005, **14**, p 196-204
10. J. Zhou, J.K. Walleiser, B.E. Meacham, and D.J. Branagan, Novel In Situ Transformable Coating for Elevated-Temperature Applications, *J. Therm. Spray Technol.*, 2010, **19**, p 950-957
11. P. Georgieva, R. Thorpe, A. Yanski, and S. Seal, An Innovative Turnover for the Wire Arc Spraying Technology, *Adv. Mater. Processes*, 2006, **8**, p 68-69
12. J.B. Cheng, X.B. Liang, B.S. Xu, and Y.X. Wu, Characterization of Mechanical Properties of FeCrBSiMnNbY Metallic Glass Coatings, *J. Mater. Sci.*, 2009, **44**, p 3356-3363
13. J.B. Cheng, Z.H. Wang, and B.S. Xu, Wear and Corrosion Behaviors of FeCrBSiNbW Amorphous/Nanocrystalline Coating Prepared by Arc Spraying Process, *J. Therm. Spray Technol.*, 2012, **21**, p 1025-1031
14. C.M. Preece and N.H. Macmillan, *Erosion, Annual Review of Materials Science*, R.A. Huggins, Ed., 1977, p 95
15. T.H. Kosel, Solid Particle Erosion, *ASM Handbook*, vol 18, ASM International, Metals Park, 1992
16. P.A. Engel, *Impact Wear of Materials*, Elsevier, Amsterdam, 1976
17. G. Jin, B.S. Xu, H.D. Wang, L. Yin, Q.F. Li, S.C. Wei, and X.F. Cui, Erosion Behavior of EEDS Cermet Coatings, *Appl. Surf. Sci.*, 2008, **254**, p 5470-5474
18. P.J. Hoop and C. Allen, The High Temperature Erosion of Commercial Thermally Sprayed Metallic and Cermet Coatings by Solid Particles, *Wear*, 1999, **233-235**, p 334-341
19. B.Q. Wang and K. Luer, The Erosion-Oxidation Behavior of HVOF Cr₃C₂-NiCr Cermet Coating, *Wear*, 1994, **174**, p 177-185
20. Y. Wang, Y. Yang, and M.F. Yan, Microstructures, Hardness and Erosion Behavior of Thermal Sprayed and Heat Treated NiAl Coatings with Different Ceria, *Wear*, 2007, **263**, p 371-378
21. E.H. Saarivirta, F.H. Stott, V. Rohr, and M. Schütze, Particle Angularity Effects on the Elevated-Temperature Erosion-Oxidation Behaviour of Aluminium Diffusion Coatings on 9% Cr Steel, *Wear*, 2006, **261**, p 746-759
22. X.Q. Yu, M. Fan, and Y.S. Sun, The Erosion-Corrosion Behavior of Some Fe₃Al-Based Alloys at High Temperatures, *Wear*, 2002, **253**, p 604-609